Perspective

MRI Quantitative Evaluation of Muscle Fatty Infiltration

Vito Chianca [1,2,*], Bottino Vincenzo [2], Renato Cuocolo [3] , Marcello Zappia [4,5,6] , Salvatore Guarino [7] , Francesco Di Pietto [8] and Filippo Del Grande [1]

1. Radiology Department EOC IIMSI, 6900 Lugano, Switzerland
2. Ospedale Evangelico Betania, Via Argine 604, 80147 Naples, Italy
3. Department of Medicine, Surgery and Dentistry, University of Salerno, 84081 Baronissi, Italy
4. Department of Medicine and Health Sciences, University of Molise, 86100 Campobasso, Italy
5. Musculoskeletal Radiology Unit, Varelli Institute, 80126 Naples, Italy
6. Campolongo Hospital, 84121 Eboli, Italy
7. Department of Radiology, Azienda Ospedaliera dei Colli, Monaldi Hospital, 80131 Naples, Italy
8. Department of Radiology, Pineta Grande Hospital, 81030 Castel Volturno, Italy
* Correspondence: vitochianca@gmail.com

Abstract: Magnetic resonance imaging (MRI) is the gold-standard technique for evaluating muscle fatty infiltration and muscle atrophy due to its high contrast resolution. It can differentiate muscular from adipose tissue accurately. MRI can also quantify the adipose content within muscle bellies with several sequences such as T_1-mapping, T_2-mapping, spectroscopy, Dixon, intra-voxel incoherent motion, and diffusion tensor imaging. The main fields of interest in musculoskeletal radiology for a quantitative MRI evaluation of muscular fatty infiltration include neuro-muscular disorders such as myopathies, and dystrophies. Sarcopenia is another important field in which the evaluation of the degree of muscular fat infiltration or muscular hypotrophy is required for a correct diagnosis. This review highlights several MRI techniques and sequences focusing on quantitative methods of assessing adipose tissue and muscle atrophy.

Keywords: MRI; DTI; T_2 mapping; radiomics; DWI

1. Introduction

In the last decade, quantitative imaging evaluation (QI) has been increasingly applied in radiological clinical practice. QI can correctly identify the pathological stages and better evaluate patients' follow-ups [1]. Magnetic resonance imaging (MRI) is the main imaging technique capable of giving quantitative information through specific sequences without ionizing radiation [2]. One of the main fields of interest for a quantitative evaluation in the musculoskeletal (MSK) system is fatty infiltration and muscle atrophy. QI evaluation quantifies muscular changes in several neuromuscular diseases such as muscular dystrophies and myopathies [3]. Moreover, with the average age increase in the world population, sarcopenia is another condition that requires a QI evaluation [4]. This is due to the direct connection with the prevalence and extent of the adipose infiltration of the locomotor muscles causing reduced muscle strength, mobility, and metabolic status changes in elderly patients [5,6]. For these reasons, it is crucial to non-invasively evaluate and monitor the state of adipose infiltration of the muscles. The measurements obtained through the use of optimized sequences allow for obtaining biomarker imaging of disease progression. In this way, it will be possible to carry out an earlier and more targeted therapy for patients.

This review article intends to overview the main quantitative MRI evaluation of adipose and muscular tissue focusing on the advantages, disadvantages, and limits of each sequence that radiologists can use during their clinical activity.

2. Chemical-Shift MR Imaging

The principle of chemical-shift imaging described by Dixon is based on different precession frequencies of fat and water protons at a specific magnetic field strength [7,8]. Two-point Dixon technique acquires two different images where proton spin magnetization vectors, at two different echo times (TE), are either in the same or in the opposite direction to each other. This acquisition allows the elaboration of in- and out-phase images [9]. Different signal intensities can then be used to generate water and fat images resulting in four different image contrasts (Figure 1). The Dixon technique provides an optimal homogeneous fat saturation and for this reason, it is preferred to other fat suppression techniques on a large field of view [10] or in areas with magnetic susceptibility for the presence of metallic components [11]. The main limitation of two-point Dixon techniques may be the B_0 heterogeneity, which causes the shift of fat and water peaks with the suppression of a wrong component; this is the so-called fat-water swapping effect that can be avoided by using unwrapping algorithms for the B_0 field heterogeneity compensation [9]. The three-point-Dixon technique is proposed to solve the limitation of the two-point-Dixon sequence. The presence of another echo acquisition with a different TE forms a complex with three equations about water content, fat content, and heterogeneity. This sequence shows a better signal-to-noise ratio (SNR) with a more homogeneous fat suppression and optimal spatial resolution [12]. Multi-echo Dixon techniques are also able to accurately quantify fat content in any voxel through fat-fraction maps where the grey value of each pixel is directly correlated with the fat infiltration [13]. Both two- or three-point Dixon sequences have been shown to quantify muscular fat fraction with excellent reliability in some anatomical areas such as rotator cuff muscles [14] or upper limbs after brachial plexus injuries [15]. Wieser et al. investigated 40 patients treated with arthroscopic rotator cuff repair with a 6-point Dixon sequence and reported a direct correlation between failed repair and the amount of fatty infiltration [16].
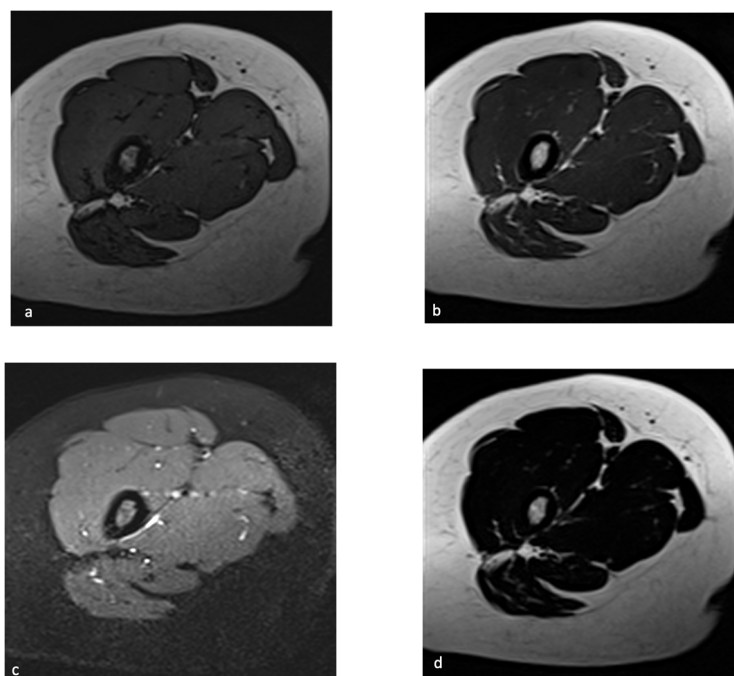
Figure 1. Dixon magnetic resonance sequence acquired on the thigh. Axial T1W out-phase (**a**), in-of-phase (**b**), 100% water images (**c**), and 100% fat images (**d**).

In the field of neuromuscular disorder, authors report that the three-point Dixon fat fraction shows a stronger correlation with a disease severity score than any other clinical tests in Duchenne muscular dystrophy patient's group [17]. Dahlqvist et al. proved that fat fraction derived by chemical-shift imaging of paraspinal muscles in facioscapulohumeral

dystrophy patients, correlated with clinical and genetic disease markers [18]. Another group used a three-point Dixon to quantify intramuscular fat fraction in Duchenne muscular dystrophy. The result shows a stronger correlation with a validated disease severity score than any other tested clinical examinations, such as isokinetic dynamometry of the knee extensor strength [17]. Another study reported higher accuracy and reliability of the three-point-Dixon sequence than conventional radiological methods for evaluating fat fractions for follow-up or therapeutic evaluation of Duchenne patients [19]. The 3D-multiple gradient-echo-Dixon sequence is reported to be a reproducible and sensitive technique able to highlight a significant difference in the fat fraction of thigh muscle, between Charcot–Marie–Tooth disease patients and volunteers [20].

3. MR Spectroscopy

MR spectroscopy (MRS) is a functional technique that provides biochemical information on human small metabolites according to their chemical-shift properties [21] on the basis of the MRS spectrum. MRS requires a high magnetic field to calculate small volumes spectra and at least 3 tesla (T) scanner is required for its higher signal-noise-ratio (SNR). Some studies reported that ultra-high magnetic field scanners (7 tesla) have advantages for MRS due to the improved SNR and the higher resolution [22,23]. Different techniques are reported for a qualitative and quantitative MRS evaluation; in particular, single-voxel or multi-voxel techniques can be used for proton MRS. Single-voxel spectroscopy (SVS) consists of the analysis of a single voxel of the selected region of interest (ROI) [24] while multi-voxel spectroscopy (MVS), is able to process simultaneously several voxels contained in a wider area [25]. Various metabolites can be differentiated depending on the MRS spectrum. In the setting of msk pathologies, phosphorus-31 (31P) MRS is used to detect metabolites containing phosphorus such as phosphocreatine, inorganic phosphate, adenosine triphosphate, and phosphocholine, which are overexpressed in case of energy consumption with related muscle changes [26,27]. Janssen et al., report that 31P-containing metabolite concentrations, measured with MRS, are strictly linked with muscle fat replacement and consequent muscle strength reduction in patients with facioscapulohumeral dystrophy [28]. However, MSK evaluation with 31P MRS requires specific hardware and software which limit its clinical use. Proton (1H) MRS does not require specialized hardware and can be easily added to a conventional MRI protocol [2]. 1H MRS can be used to measure intramuscular fatty infiltration, and some articles stated that it could represent a gold standard for noninvasive quantification of fat infiltration [29,30]. For this reason, MRS can be useful in the characterization and quantification of fat infiltration in chronic muscle pain [31], muscular dystrophies [32], or chronic myopathies [33].

The main disadvantage of the quantitative assessment of intramuscular lipid content with MRS is the significant sampling error due to the variability of the positioning of the volume of interest (VOI). Small changes in the VOI placement can determine a significant variability in fat quantification [30].

4. Relaxometry Mapping

T_2 mapping is a quantitative MR technique that measures the T_2 relaxation times of human tissues within a selected ROI [34,35]. From a technical point of view, this technique requires the acquisition of multiple images with different TEs (at least 3 different TEs) that allow the elaboration of a T_2 map [36,37]. Conventionally the T_2 map is reconstructed with fat saturation to avoid artifacts due to fatty infiltration that physiologically elevates T_2 values; so in case of fat infiltration evaluation, a T_2 map without fat suppression is mandatory [38] (Figures 2 and 3). Several acquisition methods have been proposed in the literature to evaluate T_2 values. In current clinical practice, multi-echo spin-echo sequences are typically used with various types of exponential fitting (mono-, bi-, or tri-exponential) for T_2 calculation [39]. However, these methods are sensitive to multiple confounding factors, such as B_1 inhomogeneities. Even if there are low differences in the protocol proposed by the different MR scanner vendors, the differences in the implementation of the

fitting process can be substantial. Some authors present a fast method for reconstructing T_2 maps obtained from different multi-echo spin-echo sequences and fit a method that gives reproducible results [39].
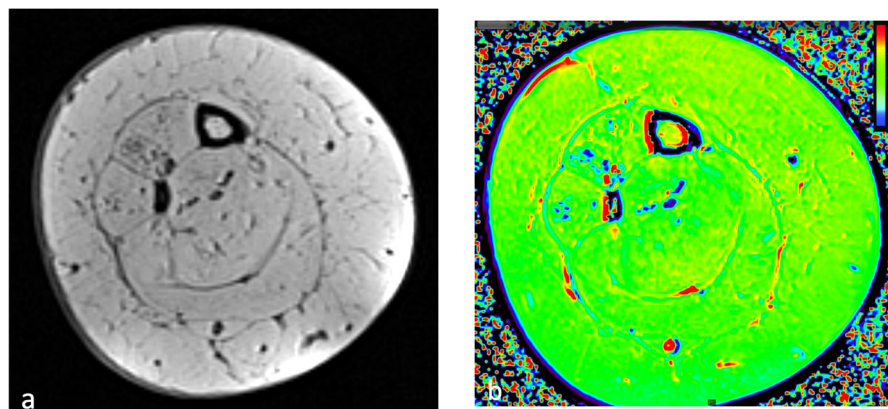

Figure 2. Axial T1w (**a**) image of a type III spinal muscular atrophy patient which shows massive fatty replacement of thigh muscles. Axial T2map image (**b**) shows very high T_2 relaxation time values of the corresponding muscle bellies. The mean T2map muscle value is 158 ms.
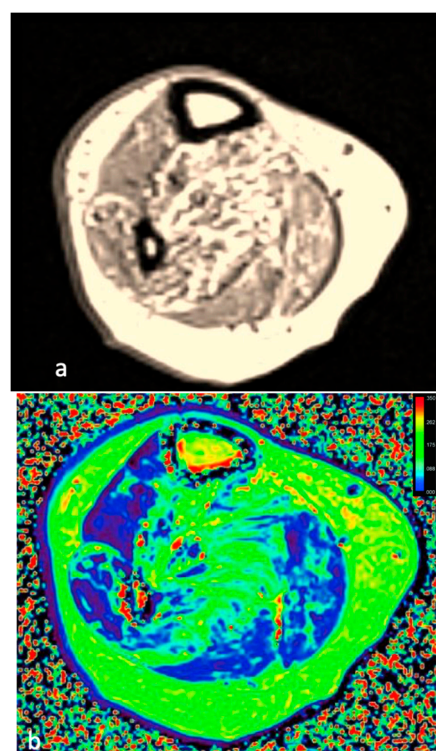

Figure 3. Axial T1w (**a**) and axial T2map (**b**) images of limb-girdle muscular dystrophy 2I patients show a partial fatty replacement of thigh muscles. The mean T2map value of muscles is 87 ms.

The correct interpretation of T_2 mapping in myopathies and dystrophies can be challenging because these patients often present edema and fatty infiltration, both conditions that elevate the T_2 values [40]. T_2 mapping remains a good support for a quantitative evaluation; however, in the literature, no defined cut-offs are described, so it is challenging to establish defined diagnostic criteria based on its values.

T_1 mapping is another method to quantify muscle fat fraction based on the modulation of T_1 values by the fat pool [41]. T_1 mapping imaging is often used to evaluate conditions related to oedema and fibrosis, where T_1 value changes reflect changes in water

mobility [42]. However, when fat is present in the voxel of interest, the resulting T_1 value is influenced by a complex of water and fat content. In the condition of fat replacement, the fat fraction amount is directly correlated with the decrease in longitudinal T_1 relaxation time [43]. Marty et al. evaluated ten healthy men and 30 men with Becker muscle dystrophy and reported high repeatability of the T_1 values measured with their high-resolution T_1 sequence able to discriminate healthy and dystrophic conditions in all the muscle groups (Student *t*-test, $p < 0.05$) [44].

Diffusion-Weighted Imaging

Diffusion tensor imaging (DTI) is an MRI-based technique evolved from the principles of DWI, which is mainly used in clinical practice for the evaluation of the central and peripheral nervous system [45–47]. DTI is based on the concept that water mobility in the human body does not move equally in all directions due to the presence of cell membranes muscle fibers or myelin sheath that restrict molecule diffusion. For this reason, water molecule diffusion is non-isotropic. For an accurate DTI sequence is mandatory to acquire DWI with high b values along at least 6 directions and a low b value DWI or a T_2-weighted sequence.

Higher b values increase gradient power and sequence diffusion weighting but reduce SNR. Authors reported an optimized sequence using 20–30 mm [3] voxel volumes, shortest TE, b values of 400–500 s/mm^2, and at least 10 gradient directions [48]. Although a clear benefit of using high b values is reported for central nervous system pathologies investigation, no articles report a definite clinical benefit of using high b values with ultra-high magnetic resonance field. About that point, Giraudo et al., use the same b value of 500 s/mm^2 on both 3 tesla and 7 tesla scanners [49]. Fractional anisotropy (FA) is the main parameter used to express fiber structural integrity; it ranges from 0 to 1; a value proximal to 1 expresses structural integrity while an FA value proximal to 0 expresses isotropic diffusion of molecules due to fiber damage [50].

Acquisition time depends mainly on the number of directions and magnetic field strength; there is a directly proportional relationship between scanning time and the number of directions, while there is an inversely proportional relationship between magnetic field strength and scanning time. Furthermore, the number of averages affects the scan time; the higher the number of averages, the longer the scan time will be. In the case of muscle evaluation 12 non-collinear directions are enough to obtain a satisfactory sequence [51]. Tractography is a DTI extension that allows 3-D visualization of muscle and nerve fibers [52,53]. Using MR with a higher magnetic field straight and higher magnetic gradients, nerve fascicle morphology and morphometric parameters can be better visualized [49].

It is possible to visualize the rarefaction of muscle fibers in the case of neurodegenerative diseases with consequent fat replacement. Klupp et al. compared paraspinal muscular DTI parameters and isokinetic dynamometer evaluation and reported a significant correlation between DTI measurements and functional tests [54].

In the setting of muscle dystrophies, Ponrartana et al. used DTI quantitative MRI parameters to evaluate Duchenne muscular dystrophy progression in the lower extremities and reported a high correlation between DTI values, and qualitative evaluation using the Mercuri grading [55]. Nevertheless, patients with a fat content of more than 45% within muscle bellies may determine an artificial decrease in ADC and a paradoxical artificial increase in FA values (Figure 4); for these reasons, progression of dystrophies positively correlates with FA and negatively with ADC values [56]. The main disadvantages of DTI are the complexity of the setup of the sequence, the scan times, and the need for a high magnetic field scanner with high-performance gradients.
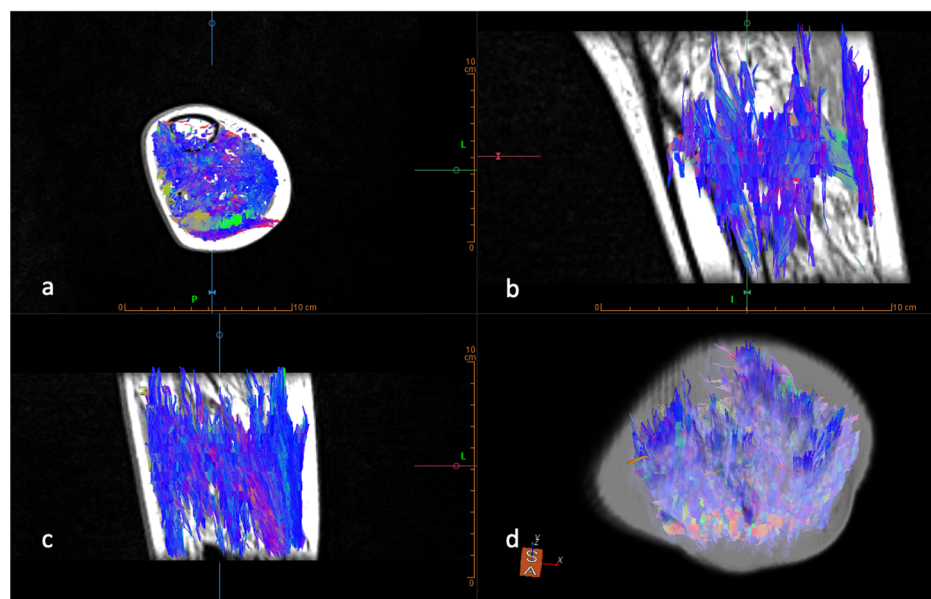
Figure 4. Axial (**a**), sagittal (**b**), coronal (**c**), and axial fusion tractography (**d**) images of a type II spinal muscular atrophy patient show rarefaction of regular muscle fibers. The DTI sequence (slice thickness: 3 mm, b value: 400, number of directions: 12) shows a mean FA value of 0.61 calculated on leg muscle compartments ROI.

Till now there were doubts about the reliability of the sequence on different scanners; Guggenberger et al. performed a wrist MR exam on 3 different 3-tesla scanners on 16 healthy volunteers and reported different FA and ADC values [57]. However, the comparison of the values with the standard deviation was small enough to not have an impact on a larger group. They also used different software for processing the values for each scanner. A recent study performed on 3 scanners (3 tesla) from different vendors, reported excellent results such as inter-vendor and inter-observer reliability using a single specific software [53].

The intravoxel incoherent motion (IVIM) is another imaging technique based on diffusion, that uses multiple b values to quantify the incoherently flowing vascular blood pool signal from that of the tissue diffusion signal [58]. IVIM reflects the water molecule's microscopic motion in each MRI voxel of the intracellular space, extracellular space, and blood capillaries [59]. With this imaging technique, diffusion and perfusion are affected by tissue characteristics such as the presence of cellular membranes, the fluid viscosity, and the velocity of perfusing spins [60]. One of the limitations of the use of this imaging method is the potential degradation of images caused by cardiac activity, and motion artifacts which limited, for years, the technique to the study of the central nervous system only [61]. However promising results were reported about the IVIM in the msk system, particularly in the differentiation of myositis from muscular dystrophy [62] or for quantification of muscle activation [63].

5. Artificial Intelligence

The use of artificial intelligence (AI) in the medical field is progressively revolutionizing the daily clinical life of physicians. AI provides an interesting tool that improves performance in all diagnostic fields [64]. AI is a field of computer science dedicated to the elaboration of systems tasks that generally require human intelligence [65]. Different subfields of AI are proposed, but the most investigated for future development are machine learning (ML) and deep learning (DL) [66]. ML trained and tested different algorithms to recognize specific image characteristics by learning processes from an origin dataset. DL is another subtype of AI based on the use of different layers of neural networks (NN) that allow a computer to analyze a large amount of data and identify useful features for a correct classification [67]. Although most AI studies in the msk field focus on tumor recognition

and classification [68–71], several authors investigated the use of AI in the evaluation of muscle fat infiltration. They reported accurate and rapid, quantitative assessment [72]. Ro et al. tested NN to automatically evaluate the occupation ratio and fatty infiltration of rotator cuff muscles on 240 patients who underwent shoulder MRI. They reported a strong negative correlation between the occupation ratio via convolutional NN and fatty infiltration via the Otsu thresholding method [73]. Regarding muscle dystrophies, Verdú-Díaz et al. collected 976 pelvic and lower limbs muscle MRIs from 10 different muscle dystrophies. They tested ML capabilities in detecting and quantifying abnormalities by comparing them with those of four specialists. The best model tested showed 95.7% accuracy, with 92.1% sensitivity and 99.4% specificity higher than the values the specialists showed [74]. Ding et al. tested AI for automated thigh muscle segmentation showing excellent accuracy and higher reproducibility in fat fraction quantification compared to manual segmentation [75].

Furthermore, ML and DL in particular are also revolutionizing other aspects of MRI in this domain, especially image acquisition and reconstruction [76]. In particular, techniques based on Generative Adversarial Networks and model-based image reconstruction from raw k space data have proven valuable to the lower acquisition time of quantitative imaging data or improve the robustness of the resulting parametric maps. As these represent two of the main current limitations for widespread clinical adoption, such technical developments may greatly aid in the clinical implementation of quantitative MRI assessment of muscle fatty infiltration.

Further research will be necessary for the clinical validation of these AI tools.

6. Conclusions

Adipose infiltration and adipose involution are important findings of inflammatory-degenerative muscle pathologies. When present, these changes indicate an advanced state of disease. MRI has multiple techniques and sequences for both qualitative and quantitative assessment such as chemical-shift sequences, spectroscopy, relaxometry, diffusion tensor imaging, and IVIM. All these sequences can calculate the degree of fat infiltration differently as shown in Table 1. However, each sequence shows some limitations that prevent their routine use in clinical practice. However, the implementation of study protocols with at least one of these sequences is necessary to obtain a tailored therapy for patients. The development of AI will allow a reduction of motion artifacts and allow to perform faster post-processing to obtain the quantitative values. For all these reasons, in modern medicine, is crucial for a radiologist to know methods for quantifying muscle fat content.

Table 1. Summary of different MR imaging techniques.

Imaging Techniques	Type of Evaluation	Disadvantages
Dixon	Quantification of muscular fat fraction with excellent reliability.	B_0 heterogeneity, which causes the shift of fat and water peaks with the suppression of a wrong component.
Spectroscopy	MRS evaluates metabolic muscle changes in case of muscle fat infiltration through the quantitative analysis of metabolites containing phosphorus.	Significant sampling error due to the variability of the positioning of the volume of interest.
Relaxometry	Quantitative relaxation time evaluation of the selected muscle.	The presence of edema determines errors in quantifying muscular fat infiltration.
DTI	Quantitative evaluation of the degree of muscular adipose infiltration by calculating the fraction anisotropy.	Complexity of the sequence setup and the scan times.
IVIM	Quantitative evaluation of the incoherently flowing vascular blood signal from that of the other tissue.	Cardiac activity and motion artifacts.

References

1. Rosenkrantz, A.B.; Mendiratta-Lala, M.; Bartholmai, B.J.; Ganeshan, D.; Abramson, R.G.; Burton, K.R.; Yu, J.-P.J.; Scalzetti, E.M.; Yankeelov, T.E.; Subramaniam, R.M.; et al. Clinical Utility of Quantitative Imaging. *Acad. Radiol.* **2015**, *22*, 33–49. [CrossRef]
2. Chianca, V.; Albano, D.; Messina, C.; Vincenzo, G.; Rizzo, S.; Del Grande, F.; Sconfienza, L.M. An update in musculoskeletal tumors: From quantitative imaging to radiomics. *Radiol. Med.* **2021**, *126*, 1095–1105. [CrossRef]
3. Forbes, S.C.; Willcocks, R.J.; Rooney, W.D.; Walter, A.G.; Vandenborne, K. MRI quantifies neuromuscular disease progression. *Lancet Neurol.* **2016**, *15*, 26–28. [CrossRef]
4. Chianca, V.; Albano, D.; Messina, C.; Gitto, S.; Ruffo, G.; Guarino, S.; Del Grande, F.; Sconfienza, L.M. Sarcopenia: Imaging assessment and clinical application. *Abdom. Radiol.* **2022**, *47*, 3205–3216. [CrossRef]
5. Marcus, R.L.; Addison, O.; Kidde, J.P.; Dibble, L.E.; Lastayo, P.C. Skeletal muscle fat infiltration: Impact of age, inactivity, and exercise. *J. Nutr. Health Aging* **2010**, *14*, 362–366. [CrossRef]
6. Messina, C.; Vitale, J.A.; Pedone, L.; Chianca, V.; Vicentin, I.; Albano, D.; Gitto, S.; Sconfienza, L.M. Critical appraisal of papers reporting recommendation on sarcopenia using the AGREE II tool: A EuroAIM initiative. *Eur. J. Clin. Nutr.* **2020**, *74*, 1164–1172. [CrossRef]
7. Huber, F.A.; Del Grande, F.; Rizzo, S.; Guglielmi, G.; Guggenberger, R. MRI in the assessment of adipose tissues and muscle composition: How to use it. *Quant. Imaging Med. Surg.* **2020**, *10*, 1636–1649. [CrossRef]
8. Chianca, V.; Cuocolo, R.; Albano, D. Editorial for "Quantification of Bone Marrow Fat Fraction and Iron by MRI for Distinguishing Aplastic Anemia and Myelodysplastic Syndromes". *J. Magn. Reson. Imaging* **2021**, *54*, 1761–1762. [CrossRef]
9. Del Grande, F.; Santini, F.; Herzka, D.; Aro, M.R.; Dean, C.W.; Gold, G.E.; Carrino, J.A. Fat-Suppression Techniques for 3-T MR Imaging of the Musculoskeletal System. *RadioGraphics* **2014**, *34*, 217–233. [CrossRef]
10. Bray, T.J.P.; Singh, S.; Latifoltojar, A.; Rajesparan, K.; Rahman, F.; Narayanan, P.; Naaseri, S.; Lopes, A.; Bainbridge, A.; Punwani, S.; et al. Diagnostic utility of whole body Dixon MRI in multiple myeloma: A multi-reader study. *PLoS ONE* **2017**, *12*, e0180562. [CrossRef]
11. Jungmann, P.M.; Agten, C.A.; Pfirrmann, C.W.; Sutter, R. Advances in MRI around metal. *J. Magn. Reson. Imaging* **2017**, *46*, 972–991. [CrossRef]
12. Lins, C.F.; Salmon, C.E.G.; Nogueira-Barbosa, M.H. Applications of the Dixon technique in the evaluation of the musculoskeletal system. *Radiol. Bras.* **2021**, *54*, 33–42. [CrossRef]
13. Kellman, P.; Hernando, D.; Shah, S.; Zuehlsdorff, S.; Jerecic, R.; Mancini, C.; Liang, Z.-P.; Arai, A.E. Multiecho dixon fat and water separation method for detecting fibrofatty infiltration in the myocardium. *Magn. Reson. Med.* **2009**, *61*, 215–221. [CrossRef]
14. Lee, S.; Lucas, R.M.; Lansdown, D.A.; Nardo, L.; Lai, A.; Link, T.M.; Krug, R.; Ma, C.B. Magnetic resonance rotator cuff fat fraction and its relationship with tendon tear severity and subject characteristics. *J. Shoulder Elb. Surg.* **2015**, *24*, 1442–1451. [CrossRef]
15. Duijnisveld, B.J.; Henseler, J.F.; Reijnierse, M.; Fiocco, M.; Kan, H.E.; Nelissen, R.G. Quantitative Dixon MRI sequences to relate muscle atrophy and fatty degeneration with range of motion and muscle force in brachial plexus injury. *Magn. Reson. Imaging* **2017**, *36*, 98–104. [CrossRef]
16. Wieser, K.; Joshy, J.; Filli, L.; Kriechling, P.; Sutter, R.; Fürnstahl, P.; Valdivieso, P.; Wyss, S.; Meyer, D.C.; Flück, M.; et al. Changes of Supraspinatus Muscle Volume and Fat Fraction After Successful or Failed Arthroscopic Rotator Cuff Repair. *Am. J. Sports Med.* **2019**, *47*, 3080–3088. [CrossRef]
17. Wren, T.A.L.; Bluml, S.; Tseng-Ong, L.; Gilsanz, V. Three-Point Technique of Fat Quantification of Muscle Tissue as a Marker of Disease Progression in Duchenne Muscular Dystrophy: Preliminary Study. *Am. J. Roentgenol.* **2008**, *190*, W8–W12. [CrossRef]
18. Dahlqvist, J.R.; Vissing, C.R.; Thomsen, C.; Vissing, J. Severe paraspinal muscle involvement in facioscapulohumeral muscular dystrophy. *Neurology* **2014**, *83*, 1178–1183. [CrossRef]
19. Wokke, B.H.; Bos, C.; Reijnierse, M.; van Rijswijk, C.S.; Eggers, H.; Webb, A.; Verschuuren, J.; Kan, H. Comparison of dixon and T1-weighted MR methods to assess the degree of fat infiltration in duchenne muscular dystrophy patients. *J. Magn. Reson. Imaging* **2013**, *38*, 619–624. [CrossRef]
20. Kim, H.S.; Yoon, Y.C.; Choi, B.; Jin, W.; Cha, J.G. Muscle fat quantification using magnetic resonance imaging: Case–control study of Charcot–Marie–Tooth disease patients and volunteers. *J. Cachex Sarcopenia Muscle* **2019**, *10*, 574–585. [CrossRef]
21. Gujar, S.K.; Maheshwari, S.; Björkman-Burtscher, I.; Sundgren, P.C. Magnetic resonance spectroscopy. *J. Neuroophthalmol.* **2005**, *25*, 217–226. [CrossRef]

22. Aringhieri, G.; Zampa, V.; Tosetti, M. Musculoskeletal MRI at 7 T: Do we need more or is it more than enough? *Eur. Radiol. Exp.* **2020**, *4*, 48. [CrossRef]

23. Wang, L.; Salibi, N.; Wu, Y.; Schweitzer, M.E.; Regatte, R. Relaxation times of skeletal muscle metabolites at 7T. *J. Magn. Reson. Imaging* **2009**, *29*, 1457–1464. [CrossRef]

24. Deshmukh, S.; Subhawong, T.; Carrino, A.J.; Fayad, L. Role of MR spectroscopy in musculoskeletal imaging. *Indian J. Radiol. Imaging* **2014**, *24*, 210–216. [CrossRef]

25. Ogg, R.; Kingsley, R.; Taylor, J. WET, a T_1- and B_1-Insensitive Water-Suppression Method for in Vivo Localized 1H NMR Spectroscopy. *J. Magn. Reson. Ser. B* **1994**, *104*, 1–10. [CrossRef]

26. Liu, Y.; Gu, Y.; Yu, X. Assessing tissue metabolism by phosphorous-31 magnetic resonance spectroscopy and imaging: A methodology review. *Quant. Imaging Med. Surg.* **2017**, *7*, 707–716. [CrossRef]

27. Leung, D.G.; Sneag, D.B.; Del Grande, F.; Carrino, J.A.; Kalia, V. Advanced MRI Techniques for Muscle Imaging. *Semin. Musculoskelet. Radiol.* **2017**, *21*, 459–469. [CrossRef]

28. Janssen, B.H.; Voet, N.B.M.; Nabuurs, C.I.; Kan, H.E.; de Rooy, J.W.J.; Geurts, A.C.; Padberg, G.W.; van Engelen, B.G.M.; Heerschap, A. Distinct Disease Phases in Muscles of Facioscapulohumeral Dystrophy Patients Identified by MR Detected Fat Infiltration. *PLoS ONE* **2014**, *9*, e85416. [CrossRef]

29. Reeder, S.B.; Cruite, I.; Hamilton, G.; Sirlin, C.B. Quantitative assessment of liver fat with magnetic resonance imaging and spectroscopy. *J. Magn. Reson. Imaging* **2011**, *34*, 729–749. [CrossRef]

30. Fischer, M.A.; Nanz, D.; Shimakawa, A.; Schirmer, T.; Guggenberger, R.; Chhabra, A.; Carrino, J.A.; Andreisek, G. Quantification of Muscle Fat in Patients with Low Back Pain: Comparison of Multi-Echo MR Imaging with Single-Voxel MR Spectroscopy. *Radiology* **2013**, *266*, 555–563. [CrossRef]

31. Ogon, I.; Takebayashi, T.; Takashima, H.; Morita, T.; Yoshimoto, M.; Terashima, Y.; Yamashita, T. Quantitative Analysis Concerning Atrophy and Fat Infiltration of the Multifidus Muscle with Magnetic Resonance Spectroscopy in Chronic Low Back Pain. *Spine Surg. Relat. Res.* **2019**, *3*, 163–170. [CrossRef]

32. Forbes, S.C.; Arora, H.; Willcocks, R.J.; Triplett, W.T.; Rooney, W.D.; Barnard, A.M.; AlAbasi, U.; Wang, D.-J.; Lott, D.J.; Senesac, C.R.; et al. Upper and Lower Extremities in Duchenne Muscular Dystrophy Evaluated with Quantitative MRI and Proton MR Spectroscopy in a Multicenter Cohort. *Radiology* **2020**, *295*, 616–625. [CrossRef]

33. Paoletti, M.; Pichiecchio, A.; Piccinelli, S.C.; Tasca, G.; Berardinelli, A.L.; Padovani, A.; Filosto, M. Advances in Quantitative Imaging of Genetic and Acquired Myopathies: Clinical Applications and Perspectives. *Front. Neurol.* **2019**, *10*, 78. [CrossRef]

34. Albano, D.; Chianca, V.; Cuocolo, R.; Bignone, R.; Ciccia, F.; Sconfienza, L.M.; Midiri, M.; Brunetti, A.; Lagalla, R.; Galia, M. T_2-mapping of the sacroiliac joints at 1.5 Tesla: A feasibility and reproducibility study. *Skelet. Radiol.* **2018**, *47*, 1691–1696. [CrossRef]

35. Chianca, V.; Albano, D.; Cuocolo, R.; Messina, C.; Gitto, S.; Brunetti, A.; Sconfienza, L.M. T_2 mapping of the trapeziometacarpal joint and triangular fibrocartilage complex: A feasibility and reproducibility study at 1.5 T. *Radiol. Med.* **2019**, *125*, 306–312. [CrossRef]

36. Staroswiecki, E.; Granlund, K.L.; Alley, M.T.; Gold, G.E.; Hargreaves, B.A. Simultaneous estimation of T_2 and apparent diffusion coefficient in human articular cartilage in vivo with a modified three-dimensional double echo steady state (DESS) sequence at 3 T. *Magn. Reson. Med.* **2012**, *67*, 1086–1096. [CrossRef]

37. Albano, D.; Bignone, R.; Chianca, V.; Cuocolo, R.; Messina, C.; Sconfienza, L.M.; Ciccia, F.; Brunetti, A.; Midiri, M.; Galia, M. T2 mapping of the sacroiliac joints in patients with axial spondyloarthritis. *Eur. J. Radiol.* **2020**, *131*, 109246. [CrossRef]

38. Arpan, I.; Forbes, S.C.; Lott, D.J.; Senesac, C.R.; Daniels, M.J.; Triplett, W.T.; Deol, J.K.; Sweeney, H.L.; Walter, G.A.; Vandenborne, K. T_2 mapping provides multiple approaches for the characterization of muscle involvement in neuromuscular diseases: A cross-sectional study of lower leg muscles in 5-15-year-old boys with Duchenne muscular dystrophy. *NMR Biomed.* **2013**, *26*, 320–328. [CrossRef]

39. Santini, F.; Deligianni, X.; Paoletti, M.; Solazzo, F.; Weigel, M.; de Sousa, P.L.; Bieri, O.; Monforte, M.; Ricci, E.; Tasca, G.; et al. Fast Open-Source Toolkit for Water T2 Mapping in the Presence of Fat From Multi-Echo Spin-Echo Acquisitions for Muscle MRI. *Front. Neurol.* **2021**, *12*, 248. [CrossRef]

40. De Mello, R.; Ma, Y.; Ji, Y.; Du, J.; Chang, E.Y. Quantitative MRI Musculoskeletal Techniques: An Update. *Am. J. Roentgenol.* **2019**, *213*, 524–533. [CrossRef]

41. Larmour, S.; Chow, K.; Kellman, P.; Thompson, R.B. Characterization of T_1 bias in skeletal muscle from fat in MOLLI and SASHA pulse sequences: Quantitative fat-fraction imaging with T_1 mapping. *Magn. Reson. Med.* **2017**, *77*, 237–249. [CrossRef]

42. Bull, S.; White, S.K.; Piechnik, S.K.; Flett, A.S.; Ferreira, V.; Loudon, M.; Francis, J.M.; Karamitsos, T.; Prendergast, B.D.; Robson, M.D.; et al. Human non-contrast T1 values and correlation with histology in diffuse fibrosis. *Heart* **2013**, *99*, 932–937. [CrossRef]

43. Murphy, W.; Totty, W.; Carroll, J. MRI of normal and pathologic skeletal muscle. *Am. J. Roentgenol.* **1986**, *146*, 565–574. [CrossRef]

44. Marty, B.; Coppa, B.; Carlier, P.G. Monitoring skeletal muscle chronic fatty degenerations with fast T_1-mapping. *Eur. Radiol.* **2018**, *28*, 4662–4668.

45. Barp, A.; Carraro, E.; Albamonte, E.; Salmin, F.; Lunetta, C.; Comi, G.P.; Messina, C.; Albano, D.; Chianca, V.; Sconfienza, L.M.; et al. Muscle MRI in two SMA patients on nusinersen treatment: A two years follow-up. *J. Neurol. Sci.* **2020**, *417*, 117067. [CrossRef]

46. Vetrano, I.G.; Sconfienza, L.M.; Albano, D.; Chianca, V.; Nazzi, V. Recurrence of carpal tunnel syndrome in isolated non-syndromic macrodactyly: DTI examination of a giant median nerve. *Skelet. Radiol.* **2019**, *48*, 989–993. [CrossRef]

47. Bäumer, P.; Pham, M.; Ruetters, M.; Heiland, S.; Heckel, A.; Radbruch, A.; Bendszus, M.; Weiler, M. Peripheral Neuropathy: Detection with Diffusion-Tensor Imaging. *Radiology* **2014**, *273*, 185–193. [CrossRef]

48. Schlaffke, L.; Rehmann, R.; Froeling, M.; Kley, R.; Tegenthoff, M.; Vorgerd, M.; Schmidt-Wilcke, T. Diffusion tensor imaging of the human calf: Variation of inter- and intramuscle-specific diffusion parameters. *J. Magn. Reson. Imaging* **2017**, *46*, 1137–1148. [CrossRef]

49. Giraudo, C.; Motyka, S.; Weber, M.; Feiweier, T.; Trattnig, S.; Bogner, W. Diffusion Tensor Imaging of Healthy Skeletal Muscles: A Comparison between 7 T and 3 T. *Investig. Radiol.* **2019**, *54*, 48–54. [CrossRef]

50. Chianca, V.; Albano, D.; Messina, C.; Cinnante, C.M.; Triulzi, F.M.; Sardanelli, F.; Sconfienza, L.M. Diffusion tensor imaging in the musculoskeletal and peripheral nerve systems: From experimental to clinical applications. *Eur. Radiol. Exp.* **2017**, *1*, 12. [CrossRef]

51. Cotten, A.; Haddad, F.; Hayek, G.; Lefebvre, G.; Dodré, E.; Budzik, J.-F. Tractography: Possible Applications in Musculoskeletal Radiology. *Semin. Musculoskelet. Radiol.* **2015**, *19*, 387–395. [CrossRef]

52. Wang, K.; Chen, Z.; Zhang, F.; Song, Q.; Hou, C.; Tang, Y.; Wang, J.; Chen, S.; Bian, Y.; Hao, Q.; et al. Evaluation of DTI Parameter Ratios and Diffusion Tensor Tractography Grading in the Diagnosis and Prognosis Prediction of Cervical Spondylotic Myelopathy. *Spine* **2017**, *42*, E202–E210. [CrossRef]

53. Chianca, V.; Albano, D.; Rizzo, S.; Maas, M.; Sconfienza, L.M.; Del Grande, F. Inter-vendor and inter-observer reliability of diffusion tensor imaging in the musculoskeletal system: A multiscanner MR study. *Insights Imaging* **2023**, *14*, 32. [CrossRef]

54. Klupp, E.; Cervantes, B.; Schlaeger, S.; Inhuber, S.; Kreuzpointer, F.; Schwirtz, A.; Rohrmeier, A.; Msc, M.D.; Hedderich, D.M.; Msc, M.N.D.; et al. Paraspinal Muscle DTI Metrics Predict Muscle Strength. *J. Magn. Reson. Imaging* **2019**, *50*, 816–823. [CrossRef]

55. Ponrartana, S.; Ramos-Platt, L.; Wren, T.A.L.; Hu, H.H.; Perkins, T.G.; Chia, J.M.; Gilsanz, V. Effectiveness of diffusion tensor imaging in assessing disease severity in Duchenne muscular dystrophy: Preliminary study. *Pediatr. Radiol.* **2015**, *45*, 582–589. [CrossRef]

56. Be, S.E.W.; Heemskerk, A.M.; Welch, E.B.; Li, K.; Damon, B.M.; Park, J.H. Quantitative effects of inclusion of fat on muscle diffusion tensor MRI measurements. *J. Magn. Reson. Imaging* **2013**, *38*, 1292–1297. [CrossRef]

57. Guggenberger, R.; Nanz, D.; Bussmann, L.; Chhabra, A.; Fischer, M.A.; Hodler, J.; Pfirrmann, C.W.; Andreisek, G. Diffusion tensor imaging of the median nerve at 3.0T using different MR scanners: Agreement of FA and ADC measurements. *Eur. J. Radiol.* **2013**, *82*, e590–e596. [CrossRef]

58. Adelnia, F.; Shardell, M.; Bergeron, C.M.; Fishbein, K.W.; Spencer, R.G.; Ferrucci, L.; Reiter, D.A. Diffusion-weighted MRI with intravoxel incoherent motion modeling for assessment of muscle perfusion in the thigh during post-exercise hyperemia in younger and older adults. *NMR Biomed.* **2019**, *32*, e4072. [CrossRef]

59. Li, Y.T.; Cercueil, J.-P.; Yuan, J.; Chen, W.; Loffroy, R.; Wáng, Y.X.J. Liver intravoxel incoherent motion (IVIM) magnetic resonance imaging: A comprehensive review of published data on normal values and applications for fibrosis and tumor evaluation. *Quant. Imaging Med. Surg.* **2017**, *7*, 59–78. [CrossRef]

60. Le Bihan, D.; Johansen-Berg, H. Diffusion MRI at 25: Exploring brain tissue structure and function. *Neuroimage* **2012**, *61*, 324–341. [CrossRef]

61. Le Bihan, D. What can we see with IVIM MRI? *Neuroimage* **2019**, *187*, 56–67. [CrossRef]

62. Ran, J.; Yin, C.; Liu, C.; Li, Y.; Hou, B.; Morelli, J.N.; Dai, B.; Li, X. The Diagnostic Value of MR IVIM and T2 Mapping in Differentiating Autoimmune Myositis From Muscular Dystrophy. *Acad. Radiol.* **2021**, *28*, e182–e188. [CrossRef]

63. Jungmann, P.; Pfirrmann, C.; Federau, C. Characterization of lower limb muscle activation patterns during walking and running with Intravoxel Incoherent Motion (IVIM) MR perfusion imaging. *Magn. Reson. Imaging* **2019**, *63*, 12–20. [CrossRef]

64. Xu, W.; Hao, D.; Hou, F.; Zhang, D.; Wang, H. Soft Tissue Sarcoma: Preoperative MRI-Based Radiomics and Machine Learning May Be Accurate Predictors of Histopathologic Grade. *Am. J. Roentgenol.* **2020**, *215*, 963–969. [CrossRef]

65. Gorelik, N.; Gyftopoulos, S. Applications of Artificial Intelligence in Musculoskeletal Imaging: From the Request to the Report. *Can. Assoc. Radiol. J.* **2021**, *72*, 45–59. [CrossRef]

66. Campagner, A.; Sconfienza, L.; Cabitza, F. H-Accuracy, an Alternative Metric to Assess Classification Models in Medicine. In *Studies in Health Technology and Informatics*; IOS Press: Amsterdam, The Netherlands, 2020; Volume 270, pp. 242–246. [CrossRef]

67. Chartrand, G.; Cheng, P.M.; Vorontsov, E.; Drozdzal, M.; Turcotte, S.; Pal, C.J.; Kadoury, S.; Tang, A. Deep Learning: A Primer for Radiologists. *RadioGraphics* **2017**, *37*, 2113–2131. [CrossRef]

68. Gitto, S.; Cuocolo, R.; Albano, D.; Chianca, V.; Messina, C.; Gambino, A.; Ugga, L.; Cortese, M.C.; Lazzara, A.; Ricci, D.; et al. MRI radiomics-based machine-learning classification of bone chondrosarcoma. *Eur. J. Radiol.* **2020**, *128*, 109043. [CrossRef]

69. Albano, D.; Cuocolo, R.; Patti, C.; Ugga, L.; Chianca, V.; Tarantino, V.; Faraone, R.; Albano, S.; Micci, G.; Costa, A.; et al. Whole-body MRI radiomics model to predict relapsed/refractory Hodgkin Lymphoma: A preliminary study. *Magn. Reson. Imaging* **2022**, *86*, 55–60. [CrossRef]

70. Chianca, V.; Cuocolo, R.; Gitto, S.; Albano, D.; Merli, I.; Badalyan, J.; Cortese, M.C.; Messina, C.; Luzzati, A.; Parafioriti, A.; et al. Radiomic Machine Learning Classifiers in Spine Bone Tumors: A Multi-Software, Multi-Scanner Study. *Eur. J. Radiol.* **2021**, *137*, 109586. [CrossRef]

71. Gitto, S.; Cuocolo, R.; Annovazzi, A.; Anelli, V.; Acquasanta, M.; Cincotta, A.; Albano, D.; Chianca, V.; Ferraresi, V.; Messina, C.; et al. CT radiomics-based machine learning classification of atypical cartilaginous tumours and appendicular chondrosarcomas. *Ebiomedicine* **2021**, *68*, 103407. [CrossRef]

72. Weber, K.A.; Abbott, R.; Bojilov, V.; Smith, A.C.; Wasielewski, M.; Hastie, T.J.; Parrish, T.B.; Mackey, S.; Elliott, J.M. Multi-muscle deep learning segmentation to automate the quantification of muscle fat infiltration in cervical spine conditions. *Sci. Rep.* **2021**, *11*, 312–329. [CrossRef]

73. Ro, K.; Kim, J.Y.; Park, H.; Cho, B.H.; Kim, I.Y.; Shim, S.B.; Choi, I.Y.; Yoo, J.C. Deep-learning framework and computer assisted fatty infiltration analysis for the supraspinatus muscle in MRI. *Sci. Rep.* **2021**, *11*, 15065. [CrossRef]

74. Verdú-Díaz, J.; Alonso-Pérez, J.; Nuñez-Peralta, C.; Tasca, G.; Vissing, J.; Straub, V.; Fernández-Torrón, R.; Llauger, J.; Illa, I.; Díaz-Manera, J. Accuracy of a machine learning muscle MRI-based tool for the diagnosis of muscular dystrophies. *Neurology* **2020**, *94*, e1094–e1102. [CrossRef]

75. Ding, J.; Cao, P.; Chang, H.-C.; Gao, Y.; Chan, S.H.S.; Vardhanabhuti, V. Deep learning-based thigh muscle segmentation for reproducible fat fraction quantification using fat–water decomposition MRI. *Insights Imaging* **2020**, *11*, 128. [CrossRef]

76. Feng, L.; Ma, D.; Liu, F. Rapid MR relaxometry using deep learning: An overview of current techniques and emerging trends. *NMR Biomed.* **2022**, *35*, e4416. [CrossRef]